RASĀYAN *J. Chem.*
Vol. 19 | No. 4 | 2307-2319 | October-December | 2026
ISSN: 0974-1496 | e-ISSN: 0976-0083 | CODEN: RJCABP
http://www.rasayanjournal.com
http://www.rasayanjournal.co.in

ENHANCED PHOTOCATALYTIC AND ANTIBACTERIAL PERFORMANCE OF GREEN-SYNTHESIZED Co_3O_4 NANOPARTICLES DERIVED FROM *Achyranthes aspera*

K. Usha[1], V. Ramesh[2], P. Koteeswari[1], D. V. Sridevi[3], and T. Kavitha[1,✉]
[1]Department of Physics, Shrimathi Devkunvar Nanalal Bhatt Vaishnav College for Women, Chromepet, Chennai600044, Tamil Nadu, India.
[2]Department of Physics and Nanotechnology, SRM Institute of Science and Technology, Kattankulathur, Chengalpattu 603203, Tamil Nadu, India.
[3]Department of Chemistry, Saveetha School of Engineering, Saveetha Institute of Medical and Technical Sciences, Tandalam, Chennai 602105, Tamil Nadu, India.
✉Corresponding author: kavithatphd@gmail.com

ABSTRACT

In this study, Co_3O_4 nanoparticles (NP's) were synthesised using *Achyranthes aspera* leaf extract via a sol-gel method, and the prepared material's structural, photocatalytic and antibacterial properties have been analysed. The cobalt sulfate hexahydrate ($CoSO_4 \cdot 6H_2O$) was mixed with the leaf extract under controlled conditions, then calcined. Characterisation techniques, including XRD, FTIR, UV-DRS, SEM, TEM, and EDX, confirmed the nanoparticles' (NPs) structural and optical properties. XRD analysis acknowledged the construction of a cubic spinel structure. SEM revealed a flake-like structure (morphology) with particle sizes calculated to be ~8.7 to 319.9 nm, while TEM indicated a spherical shape. UV-DRS analysis showed two band gaps at 3.5 eV and 4.24 eV, calculated by the Tauc relation. The photocatalytic performance of Co_3O_4 NPs exhibited degradation efficiencies of 58% under sunlight and 62% in a photoreactor. Antibacterial activity, evaluated using the resazurin assay, demonstrated significant inhibition of bacterial growth. MIC values of 62.5 µg/mL were recorded for *Staphylococcus aureus* and *Enterococcus faecalis*, underscoring their efficacy against Gram-positive bacteria. These aforementioned findings demonstrate the potential uses of Co_3O_4 NPs in environmental domains, especially in antibacterial therapies and water purification. These results show that green-synthesised Co_3O_4 NPs are an economical and environmentally sustainable nanomaterial for antibacterial and wastewater remediation applications. By combining environmentally friendly synthesis with multipurpose environmental applications, the study advances green nanotechnology and provides a strong basis for further investigation into sustainable photocatalysts and antimicrobial nanomaterials. Additionally, by promoting sustainable technology for environmental preservation and water purification, the current initiative directly advances SDG-6: Clean Water and Sanitation.

Keywords: *Achyranthes aspera*, Cobalt Oxide Nanoparticles, Green Synthesis, Sol-Gel Method, Photocatalysis, Antibacterial Activity, Methylene Blue Degradation, Photoreactor.

RASĀYAN *J. Chem.*, Vol. 19, No.4, 2026

INTRODUCTION

Nanotechnology is a rapidly advancing field that has witnessed significant development in recent years. Among the various types of nanoparticles that have emerged, metal oxide nanoparticles have proven to be particularly crucial due to their remarkable properties and diverse applications.[1] Cobalt oxide (Co_3O_4) NP's have attracted extensive attention due to their excellent physicochemical properties and their extensive applications in photocatalysis, antimicrobial therapies, and environmental remediation. Recent studies underscore the growing importance of developing environmentally sustainable synthesis methods for Co_3O_4nanoparticles, especially as global efforts increasingly focus on advancing sustainable technologies.[2] Conventional techniques for creating metal oxide nanoparticles often involve hazardous chemicals and energy-intensive processes that are detrimental to the environment.[3] Green synthesis methods using plant extracts have become viable alternatives to address these issues. As emphasised in extensive studies, green synthesis methods align with the principles of sustainable chemistry, offering benefits such as affordability, biocompatibility, and reduced environmental impact.[4] The sol-gel method,

This work is licensed under a CC BY 4.0 license.

especially when paired with plant-based reducing agents, is effective for synthesising Co_3O_4 nanoparticles.[5] Research has shown that this approach enables enhanced control over particle size, shape, and crystallinity while retaining the advantages of green chemistry principles. The method's adaptability and reproducibility make it especially ideal for large-scale applications.[6] *Achyranthes aspera* is a member of the Amaranthaceae family that grows in tropical and subtropical climates, including India and Pakistan. This medicinal herb, often referred to as the "prickly chaff flower," has been widely used in traditional medicine systems for its diverse pharmacological properties.[7] The plant parts are used to treat illnesses such as rheumatoid arthritis, urinary tract infections, pneumonia, and upper respiratory infections.[8] Furthermore, its bioactive components make it useful against a variety of sexually transmitted infections caused by bacteria and fungi. Historical sources suggest its use in Ayurvedic medical formulations such as Rasa, Guna, and Vipaka.[9] *Achyranthes aspera's* medicinal significance includes uses for fever, dysentery, and skin problems. The plant also has anti-inflammatory, rheumatic, and antileprotic effects. It is a hot-water extract that alleviates arthritis pain, and dried leaf powder combined with honey has been shown to help in the initial stages of asthma.[10,11] Fresh leaf paste can be applied topically to relieve discomfort from bug bites, and its decoctions are used to treat diarrhoea, dysentery, and rabies. It also has tranquillising qualities and has been linked to cardiovascular and spermicidal advantages.[12] Because of its many medicinal uses, *Achyranthes aspera* is a great choice for applications via green synthesis. As a biological reducing agent, this medicinal herb has demonstrated exceptional promise. Flavonoids, alkaloids, and polyphenols are among the bioactive substances found in the plant's leaves that aid in the stabilisation and reduction of metal ions during the creation of nanoparticles. These substances may improve the biological activities of nanoparticles in addition to aiding in their production.[13] Photocatalytic uses of Co_3O_4 nanoparticles have received significant interest in environmental restoration efforts.[14] According to studies, these nanoparticles have excellent photocatalytic activity for degrading organic contaminants under both UV and visible light conditions. Co_3O_4 NP's have a large surface area and peculiar electronic characteristics, leading to improved photocatalytic activity.[15] Green-synthesized Co_3O_4nanoparticles show promise for antimicrobial applications.[16] According to research, these nanoparticles have robust antibacterial action on both '*gram-positive and gram-negative bacteria'*, which makes them potentially useful in a variety of biological applications. The antibacterial process is ascribed to the formation of reactive O_2 species and the NP's capacity to interact with bacterial cell membranes.[17] Characterisation of Co_3O_4 nanoparticles is essential for understanding their characteristics and optimising their applications. Modern analytical techniques, including P-XRD, scanning SEM, TEM, and UV-visible spectroscopy, provide valuable data on the crystal structure, surface morphology, and UV-optical properties of these nanomaterials.[18] Combining the sol-gel technique with *Achyranthes aspera* leaf extract is a unique way for green manufacturing of Co_3O_4 nanoparticles.[19] This technology not only ensures environmental sustainability but also has the potential to improve nanoparticle functional characteristics by incorporating bioactive components from plant extracts.[20] The development of environmentally sustainable synthesis routes that simultaneously provide controlled particle morphology, improved photocatalytic efficiency, and broad-spectrum antibacterial activity remains a significant challenge, despite the growing number of reports on the green synthesis of Co_3O_4 nanoparticles. The application of Achyranthes aspera leaf extract as a biogenic reducing and stabilising agent in the sol-gel manufacture of Co_3O_4 nanoparticles, in particular, has received little attention. There are currently insufficient thorough investigations demonstrating the connection between their physicochemical properties and multifunctional performance. In order to close this research gap, the current study uses an environmentally benign sol-gel method to create Co_3O_4 nanoparticles using leaf extract from Achyranthes aspera. XRD, UV-DRS, FT-IR, SEM-EDS, and TEM analyses were used to examine the structural, optical, and morphological properties of the generated nanoparticles. Methylene blue dye degradation under solar radiation was used to test the materials' photocatalytic activity, and their antibacterial effectiveness against both Gram-positive and Gram-negative bacterial pathogens was investigated. Green chemistry and multifunctional nanomaterials work together to create a sustainable approach to biomedical applications and environmental cleanup. Additionally, this work directly supports the Sustainable Development Goals (SDGs) of the United Nations, particularly SDG 6 (Clean Water and Sanitation) through photocatalytic wastewater treatment, SDG-12 (Responsible Consumption and Production)

through sustainable nanoparticle synthesis, and SDG-3 (Good Health and Well-Being) through the development of environmentally friendly antimicrobial nanomaterials. The findings have important ramifications for the development of green nanomaterials for environmentally and medically sustainable technologies.

EXPERIMENTAL

Materials and Methods

Every compound used in this study was of analytical purity and was used without further purification. Sodium hydroxide (NaOH) was utilised to adjust pH and precipitate cobalt ions, while cobalt sulfate hexahydrate ($CoSO_4 \cdot 6H_2O$) was utilised as a cobalt precursor. In order to produce Co_3O_4 nanoparticles in an environmentally friendly manner, fresh leaves of Achyranthes aspera were collected and utilised as natural reducing and stabilising agents. Methylene blue (MB) dye was used as the model organic pollutant in the photocatalytic studies. Resazurin dye was used as a metabolic indicator in antibacterial investigations. Dimethyl sulfoxide (DMSO) and streptomycin were used as positive and negative controls, respectively. De-ionised water was used for all experimental procedures.

Green Synthesis of Co_3O_4 Nanoparticles

Using Achyranthes aspera leaf extract as a natural reducing and stabilising agent, Co_3O_4 nanoparticles were prepared using the green sol-gel method. To extract bioactive phytochemicals, 50 g of fresh leaves were thoroughly washed, chopped into small pieces, and refluxed with 100 mL of deionised water at 70–80°C. The extract was stored for later use after being filtered twice with nanofilter paper. A homogeneous cobalt precursor solution was obtained by dissolving 8 g of $CoSO_4 \cdot 6H_2O$ in 100 mL of deionised water while stirring constantly. The generated leaf extract was then gradually added in 20 mL. After that, an alkaline pH and cobalt hydroxide precipitation were attained by gradually adding an aqueous solution of 4 g NaOH in 100 mL of deionised water (DI). To finish the reaction, the reaction mixture was continuously stirred for a full day. To obtain black crystalline Co_3O_4 nanoparticles, the precipitate was repeatedly cleaned with deionised water, dried at 80 °C for two hours, and then calcined at 450 °C for two hours. For additional characterisation and application investigation, the calcined product was ground into a fine powder. Fig. 1 shows a schematic representation of the synthesis process.

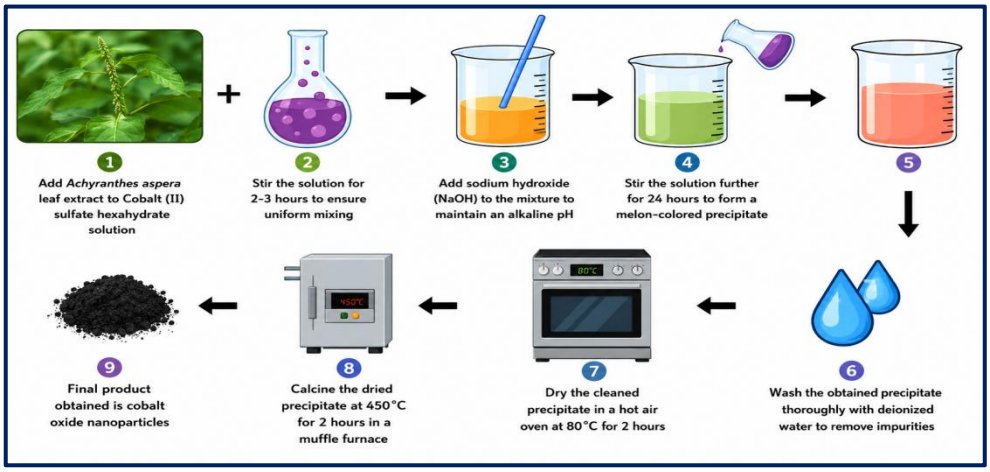


Fig.-1: Schematic Representation of the Sol-Gel Synthesis Process for Cobalt Oxide (Co_3O_4) Nanoparticles

Characterization of Co_3O_4 NPs

An experiment was carried out to examine the shape and optical characteristics of the generated green Co_3O_4 nanoparticles. Using Cu Kα radiation (λ = 1.5418 Å) on a SmartLab SE X-ray (Rigaku, Japan), powder X-ray diffraction (XRD) was used to confirm the produced Co_3O_4 crystal phases. A Shimadzu IRAffinity-1 FT-IR spectrophotometer operating in the KBr pellet mode was used to perform functional group analysis. A UV-vis Spectrophotometer in Diffuse Reflectance mode (DRS) using a Jasco V650 with ISV722 in the 200–800 nm range was used to measure the optical band gap of the generated Co_3O_4 NPs. SEM using an EDX analyser on a TESCAN VEGA3 SBH at 30kV was used to perform morphological and elemental analyses utilising tungsten filaments as the electron source. An FEI Tecnai

G2 20 S-TWIN TEM running at 200 kV with a LaB6/W emitter as the electron source was used to examine surface morphology. The Lakeshore VSM 7410 Vibrating Sample Magnetometer (VSM) was used to measure the magnetic characteristics of the as-synthesised NPs at room temperature (RT).

Photocatalytic Activity of Co_3O_4 Nanoparticles

MB dye was used to investigate the photocatalytic activity of green-produced nanoparticles. A 2 mM dye solution was added to 50 mL of Co_3O_4 NPs at room temperature. To achieve adsorption-desorption on the catalyst, this suspension was agitated for thirty minutes and stored in a dark place. Following filtration, the sample was analysed at 664 nm with a UV-visible spectrophotometer to assess the dye residue concentration. MB's decolourisation was accomplished by maintaining the solution in photoreactors that produced both visible and indirect sunlight. The absorbance was measured every ten minutes with a UV-visible spectrophotometer to trace the degradation of the MB dye. Optimisation tests were conducted to determine the optimal catalyst dose, dye concentration, and photocatalytic degradation time for MB. The degradation efficiency was estimated by comparing the initial and final absorbance after a specified period. The MB degradation percentage was approximated using the equation below[21]:

$$\text{Degradation efficiency } (\%) = \left[\frac{C_0 - C_t}{C_0}\right] \times 100 \quad (1)$$

Where C_t represents the present concentration of MB, while C_0 represents the initial concentration, after a 30-minute adsorption–desorption equilibrium.

Antibacterial Activity of Co_3O_4 Nanoparticles

The minimal inhibitory concentration (MIC) was determined using the standard broth microdilution technique. This was further confirmed using the resazurin assay. The antibacterial efficacy of *Achyranthes aspera*-mediated Co_3O_4 nanoparticles was assessed in a 96-well microtitre plate under aseptic conditions. In the first well, 100 µL of the as-synthesized NP's solution was added, followed by a serial dilution using 50 µL of nutrient broth in the subsequent wells. Each well was then inoculated with 10 µL of bacterial suspension and 10 µL of resazurin indicator. The sample plate was incubated and incubated at 37°C for 24 hours, after which the results were analysed based on colourimetric changes.

RESULTS AND DISCUSSION

PXRD Analysis of Co_3O_4 Nanoparticles

The crystallographic planes (220), (311), (400), (511), and (440) were assigned to the diffraction peaks at 2θ = 31.42°, 36.99°, 45.11°, 59.49°, and 65.54°, respectively. These peaks verified the formation of a face-centred cubic (FCC) spinel Co_3O_4 in good accordance with JCPDS Card No. 42-1467.[22] The effectiveness of Achyranthes aspera leaf extract as a natural reducing and stabilising agent is demonstrated by the lack of additional diffraction peaks, which shows that no further cobalt oxide phases or impurities were generated during green synthesis. The successful production of nanocrystalline Co_3O_4 is indicated by the average crystallite size, which was found to be approximately 23 nm using the Scherrer equation. These nanoscale crystallites provide more active surface sites and a larger specific surface area, which are beneficial for antibacterial activity and photocatalytic activity.

Saba Naz *et al.*[23] observed similar crystallite sizes for the green-produced Co_3O_4 nanoparticles, confirming the reliability of the suggested synthesis method. Equations (2-4) were used to estimate the crystallographic parameters, including average crystallite size (D), lattice constant (a), two successive plane spacing (d), and dislocation density (δ). 8 g of $CoSO_4.6H_2O$ were dissolved in 100 mL of deionised water while being continuously stirred to create a homogeneous cobalt precursor solution. The generated leaf extract was then gradually added in 20 mL. After that, an alkaline pH and cobalt hydroxide precipitation were attained by gradually adding an aqueous solution of 4 g NaOH in 100 mL of DI water. At the end of the reaction, the mixture was continuously stirred for a full day.

To obtain black crystalline Co_3O_4 nanoparticles, the precipitate was repeatedly cleaned with DI water, dried at 80 °C for 2 hours, and then calcined at 450 °C for two hours. For additional characterisation and application investigation, the calcined product was ground. Figure-1 shows a schematic representation of the synthesis process.

$$D = \frac{K_\alpha \lambda}{\beta Cos(\theta)} \quad (2)$$

$$a_0 = \frac{d_{hkl}}{\sqrt{h^2+k^2+l^2}} \quad (3)$$

$$\delta = \frac{1}{D^2} \quad (4)$$

Where K is a shape factor for Shcherr equation (0.94), λ is the wavelength of X-Ray used in XRD (λ = 1.5418 Å), θ is the diffraction angle in degree, β is the FWHM (full-width half maximum) due to the crystallite dimensions (Masoud *et al*., 2014),[24] a_0 is the cubic lattice constant, δ is the dislocation density, d_{hkl} is the interplanar spacing and hkl is Miller indices.[25] Our study's findings indicate that the average d spacing value is 2.0428 nm and the average crystal size is 23 nm. By comparing these results to the JCPDS card, we can see that the standard lattice constant is 8.3515, whereas the predicted lattice constant for our crystal is 7.56064. The difference between the two values is just 0.7986, showing that the standard and computed values of the lattice constant are close. This (Fig.-2) suggests the crystal structure is cubic. The important crystal planes are listed in Table-1.

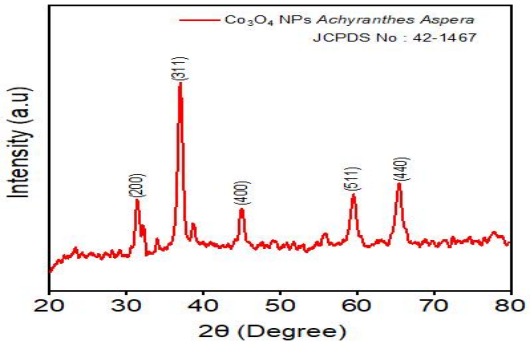


Fig.-2: XRD Analysis of Synthesised Co_3O_4 NPs

Table-1: List of the Important Crystalline Parameters of Co_3O_4 NPs

Peak Position 2θ (°)	(*hkl*)	FWHM β (°)	Lattice constant (a) Å	Interplanar distance (d) Å	Crystallite-Size D (nm)	Dislocation density (δ)
31.42	*(200)*	0.167598	5.60203	2.80101	51.49	0.00037714
36.99	*(311)*	0.761470	8.05277	2.42800	11.49	0.00075745
45.11	*(400)*	0.240383	8.03244	2.00806	37.38	0.00071582
59.49	*(511)*	0.659940	8.03571	1.54647	14.50	0.00044756
65.54	*(440)*	2.693257	8.08439	1.42843	03.66	0.00074721
Average values			7.56064	2.04280	23.70	0.00060904

FT-IR and UV Optical Studies of Co_3O_4 Nanoparticles

FTIR spectroscopy measurements identified and confirmed that the key functional groups are enabled for the reduction and stabilization of Co_3O_4 NPs' as shown in Fig.-3. Prominent peaks observed at 553 cm^{-1} and 659 cm^{-1} confirm the presence of Co_3O_4, where the intensity-peak at 659 cm^{-1} corresponds to Co(III)-O vibrations, and the intensity-peak at 553 cm^{-1} is attributed to Co–O stretching vibrations.[26,27] The absorption band at 1129 cm^{-1} is associated with C–O stretching vibrations.[28] The two most significant peaks at 1652 cm^{-1} and 1400 cm^{-1} correspond to the asymmetric and symmetric stretching vibrations (C=O) of the carboxylate group, respectively.[29] The peak at 2358 cm^{-1}, observed in calcined samples at 350 °C and 400 °C, falls within the range of 1800–2500 cm^{-1} and is linked to the C–H stretching modes of organic residues.[30] The broad band centered at 3435 cm^{-1} is attributed to O-H stretching vibrations, indicating the presence of hydroxyl groups.[31] Our findings reveal the existence of functional groups that enhance both the catalytic activity and stability of Co_3O_4 nanoparticles. By leveraging the advantages of

green synthesis and addressing existing gaps in functional group identification, this study represents a significant advancement over current literature. The identification of alkynes, amines, alkyl halides, alcohols, and phenols on the nanoparticle surface suggests enhanced surface functionality, which is expected to improve catalytic efficiency in various applications.

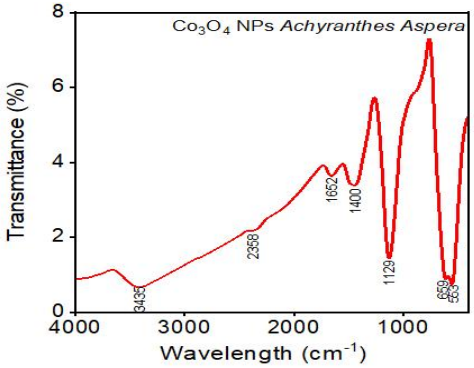


Fig.-3: FT-IR Spectrum of Green-Synthesised Co_3O_4 NPs

The UV-DRS analysis revealed that Co_3O_4 NPs exhibit strong light absorption in the visible region, as shown in the spectrum. Figure-4a shows characteristic absorption peaks of Co_3O_4 NPs in the wavelength ranges of 200-350 nm and 380-600 nm, with notable absorption maxima at approximately 250 nm and 400 nm.[32] This optical property is predominantly advantageous for photocatalytic applications, as it enables the material to effectively utilise visible light. The optical bandgap (E_g) of the Co_3O_4 NPs was estimated using Tauc's equation (5), which relates the absorption coefficient (α) and photon energy (hν) for a straight-line slope method.[33]

$$Eg = (\alpha h\nu)^n = A\ (h\nu - E_g) \qquad (5)$$

Where E_g is the optical bandgap energy, n = 2 is the indirect allowed transition, ν is the light frequency, α is the coefficient of light absorption, and h is Planck's constant (6.626×10^{-34} Js).[34] Optical characteristics of Co_3O_4 nanoparticles revealed the presence of two band gaps: 3.5 eV and 4.24 eV, as shown in Fig.-4b. The two bandgap estimates change between 3.4 eV and 4.3 eV as the surfactant concentration increases. This intriguing property may be related to the well-known phenomenon of scaling down semiconductor particles to a few nanometers, as illustrated in the image. As a result, the energy bandgap might be attributed to the lower particle sizes in the samples. The values are consistent with the preceding literature.[35-37]

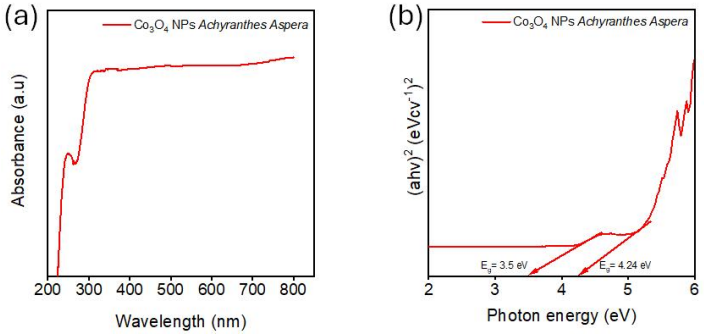


Figure 4. UV-DRS Spectrum and Fig.4b. Tauc Plot of Green-Synthesised Co_3O_4 NP

TEM and SEM Microscopic Studies of Co_3O_4 Nanoparticles

The characteristics and size distribution (morphology) of Co_3O_4 NPs are illustrated in the TEM micrographs, as shown in Fig.-5(a-c). The particles appear predominantly spherical and are dispersed across various magnifications.[38] High-resolution TEM (HR-TEM) analysis has shown well-defined lattice fringes, which confirms the high crystallinity of the synthesised Co_3O_4 NPs. The interplanar spacing measured at 0.243 nm corresponds to the (311) plane of the cubic spinel Co_3O_4 phase, consistent with standard X-ray crystallographic data. The particle size, as determined from HR-TEM images, ranges from

18 to 50 nm, which aligns well with the average crystallite size of approximately 23 nm estimated from XRD analysis.[39] The surface morphology and structural features of the Co_3O_4 nanoparticles are further examined through SEM images, as shown in Fig.-5(d-f). For the sample calcined at 450 °C, particle sizes derived from SEM micrographs using ImageJ software were 8.7 nm, 31.6 nm, 41 nm, 76.4 nm, 143.6 nm, and 319.9 nm.

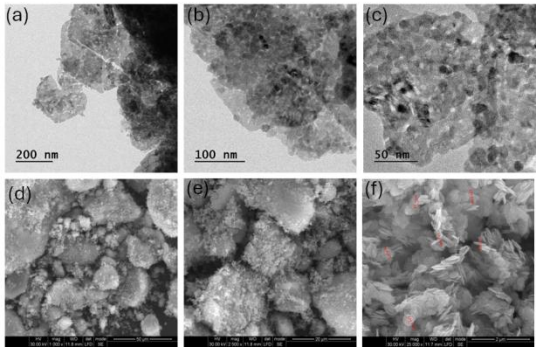


Fig.-5(a-c): Illustrations of TEM and Fig.-5(d-f): SEM Micrographs in Various Magnifications

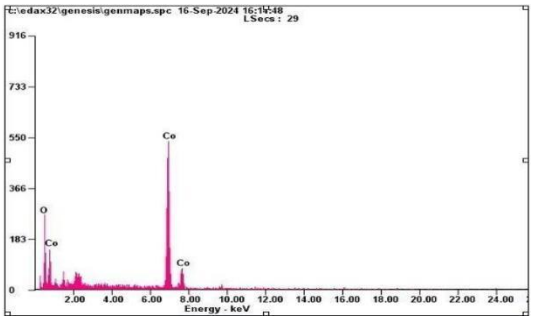


Fig.-5g: EDX Analysis of Green-Synthesised Co_3O_4 NPs

Table 2: The EDX Analysis of Green-Synthesised Co_3O_4 NPs.

Element	Wt.%	At. %
OK	30.31	61.57
CoK	69.69	38.43
Matrix	Correction	ZAF

The SEM analysis clearly shows that the NPs are aggregated into flake-like structures with distinct boundaries.[40,41] Furthermore, the presence of various chemical compounds was confirmed by elemental analysis (Fig.-5g), summarised in Table-2, indicating that oxygen comprises 30.31 Wt.% and 61.57 At. %, while cobalt accounts for 69.69 Wt.% and 38.43 At.%. This elemental composition aligns with the expected stoichiometry of the spinel Co_3O_4 phase. The high cobalt content confirms its structural dominance, and the oxygen distribution highlights its essential role in maintaining the integrity of the spinel lattice.

Magnetic Properties of Co_3O_4 Nanoparticles

Utilising a vibrating sample magnetometer (VSM), the magnetic properties of Co_3O_4 NPs were evaluated for an entire cycle between -1.5 T and 1.5 T at ambient temperature. The results are depicted in Fig.-6. The applied magnetic field was between -10000 and +10000 Oe. Coercivity and retentivity measurements of the as-synthesised nanoparticles showed magnetic field hysteresis at H_c =118.55 Oe and M_r = 68.43 emu/g. The sample's mild ferromagnetic behaviour was confirmed by the saturation magnetisation M_s, which was determined to be 38.08 emu/g.[42] Weak ferromagnetism is also characterised by the sample's higher coercivity.[43] Uncompensated surface spins and/or finite-size effects are responsible for the weak ferromagnetic character of Co_3O_4NPs.[44] It is commonly recognised that the size, shape, and crystallinity of NPs have a significant impact on their magnetic properties.[45] TEM studies, however, show that the material has a cubical form with great crystallinity. The VSM analysis validates the TEM results.

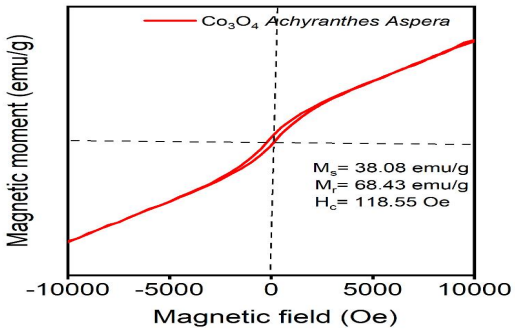


Fig.-6: Illustrates the Vibrating Sample Magnetometer for Co_3O_4 *Achyranthes Aspera* NPs'

Photocatalytic Activity of Co_3O_4 Nanoparticles

The photodegradation of MB dye by Co_3O_4 NPs after two hours of calcination at 450 ˚C, as depicted in Fig.-7a. Its rate constant in the first-order rate law is $1.59\times10^{-2}min^{-1}$, or 0.0159 min^{-1}. Its regression coefficient value is an excellent $R^2 = 0.873$ (Fig.-7b). The investigation of MB dye degradation using UV-visible spectroscopy revealed that Co_3O_4 NPs exhibited 62% photocatalytic activity within 60 minutes (Fig.-7c). The efficacy of the Co_3O_4 photocatalyst in the photoreactor was 62%. Still, in direct sunshine, it was 58%. When the original dye concentration increases, the percentage degradation efficiency decreases for two reasons. The exact dosage of photocatalyst produces hydroxyl radicals, but this production does not rise proportionately as the starting concentration of MB rises, resulting in a relatively lower OH concentration. Second, fewer photons reach the photocatalyst surface when the amount of light absorbed by the dye molecules increases.[46] The direct photocatalytic activity was analysed by demonstrating that light, superoxide radicals, and hydroxyl radicals all played a role in the degradation of the MB dye. When a photocatalyst absorbs sunlight with energy (hν) equal to or greater than the band gap energy (Eg), it generates an electron-hole pair. The equations (6-12) illustrate this process, which entails stimulating an electron to move from the valence band (VB) to the conduction band (CB), leaving a hole in the valence band.[47]

$$Co_3O_4\ (NPs) + h\cup \rightarrow Co_3O_4\ NPs\ (e^-_{CB}) + Co_3O_4\ NPs\ (h^+_{VB}) \quad (6)$$

$^{\bullet}OH$ radicals are created when water molecules join forces with holes. However, as demonstrated by the sequence of events,[48,49] the O_2 scavenges the electrons and transforms into *OH via the HOO* and H_2O_2 intermediates.

$$Co_3O_4\ (e^-_{VB}) + O_2 \rightarrow O^{\cdot}{}_2^- \quad \text{(Superoxide radical)} \quad (7)$$

$$O^{\cdot}{}_2^- + H_2O \rightarrow HOO^{\cdot} + OH^- \quad (8)$$

$$2HOO^{\cdot} \rightarrow H_2O_2 + O_2 \quad (9)$$

$$H_2O_2 + O^{\cdot}{}_2^- \rightarrow OH^{\cdot} + OH^- + O_2\ \ [OH^{\cdot} \rightarrow \text{Hydroxyl radical}] \quad (10)$$

$$Co_3O_4\ (h^+_{CB}) + H_2O \rightarrow OH^{\cdot} + Co_3O_4 \quad (11)$$

$$MB + {}^{\bullet}OH \rightarrow CO_2 + H_2O \quad (12)$$

The superoxide radical is created when a free electron reacts with molecular oxygen. Strong oxidising agents like OH. Break down organic molecules non-selectively, producing innocuous byproducts like CO_2 and H_2O. Additionally, several bimolecular substances found in plant extracts and even on the surface of nanoparticles operate as catalysts to enhance photocatalytic activity and the degradation of dye molecules. Table-3 shows the degradation response to different photocatalysts.[50,51]

The green-produced Co_3O_4 nanoparticles may be used for sustainable wastewater management and support SDG-6 (Clean Water and Sanitation), as demonstrated by the increased efficiency of photocatalytic degradation of methylene blue (MB dye). Achyranthes aspera is produced through resource-efficient synthesis of nanomaterials using leaf extract-mediated green synthesis, which is devoid of dangerous reducing chemicals and compliant with SDG-12 (Responsible Consumption and Production).

Antibacterial Activity of Co_3O_4 Nanoparticles

Microbial infections have posed significant health challenges to both humans and animals since ancient times. Among these, bacterial diseases contribute substantially to global morbidity and mortality.[52] The

increasing prevalence of antimicrobial resistance has exacerbated this issue, necessitating the search for novel antimicrobial agents.[53]

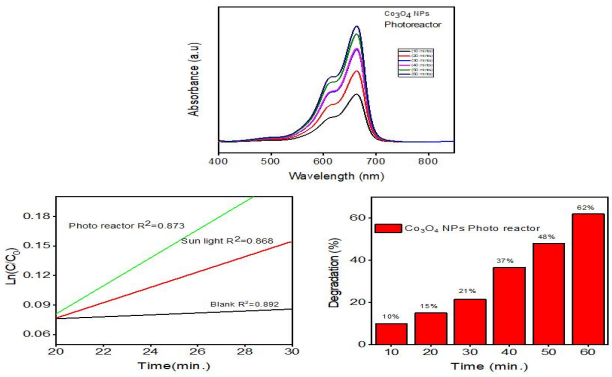


Fig.-7a: UV Absorption Spectra for MB Dye Solution Using Co_3O_4 NPs, Fig.-7b: Pseudo-First-Order Co_3O_4 NPs, and Fig.-7c: with C/C_0 vs. Time Plots for Photocatalytic Dye Degradation of MB Solution

Table-3: Shows the Degradation Response to Different Photocatalysts

Material	Degradation	References
Tio_2 Nanotubes	48.2%	[44]
$ZnCo_2O_4$ NPs	RhB→ 38 % CR →61%	[45]
Co_3O_4 NPs	MB Photoreactor: 62 % Sunlight: 58%	Present Work

Nanoparticles, particularly those synthesised through biogenic pathways, have shown promising antibacterial properties against a variety of bacterial strains.[54] The Co_3O_4 NPs have gained widespread attention due to their structural, biomedical, and antibacterial activities.[55] The present study investigates the antibacterial efficacy of Co_3O_4 NPs synthesised using *Achyranthes aspera* leaf extract. Studies have demonstrated the antibacterial activity of Co_3O_4 NPs against a wide range of microbial pathogens.[56] Table-4 lists *Pseudomonas aeruginosa, Staphylococcus aureus, Escherichia coli, and Enterococcus faecalis,* which were used to evaluate the antibacterial activity of Co_3O_4 NPs, and the corresponding MIC values of the microorganisms are listed in Table-5. The nanoparticles synthesised in this study exhibited minimum inhibitory concentration (MIC) values of 62.5 µl against Gram-positive bacteria, including *Staphylococcus aureus* and *Enterococcus faecalis*. For Gram-negative bacteria, MIC values were 125 µl for *Pseudomonas aeruginosa* and 250 µl for *Escherichia coli*. The antibacterial activity of Co_3O_4 NPs is primarily attributed to their electrostatic interaction with bacterial surfaces, leading to cell wall disruption. This interaction increases membrane permeability and promotes the generation of reactive oxygen species (ROS), resulting in oxidative stress and microbial inhibition.[57] ROS generation is a key antibacterial mechanism, involving the production of superoxide radicals (O^{2-}), hydroxyl radicals (OH·), hydrogen peroxide (H_2O_2), and singlet oxygen (O_2), each exerting varying degrees of antimicrobial action. Notably, hydroxyl radicals and singlet oxygen can induce acute bacterial death, while superoxide radicals and hydrogen peroxide may be neutralised by endogenous antioxidant enzymes.[58] The antibacterial activity of Co_3O_4 NPs (Fig.-8) follows multiple mechanisms, including electrostatic interactions causing mechanical damage to bacterial cell walls, ROS-mediated oxidative stress, and disruption of protein activities and cell structures due to metal cation release. These nanoparticles can also interfere with bacterial metabolic pathways, leading to pore formation in cell membranes and inhibition of cellular growth.[59] Additionally, antimicrobial activity has been observed in phenolic compounds, which alter membrane permeability, disrupt oxidative phosphorylation, and inhibit active transport, leading to loss of metabolite.[60] MIC values indicate the lowest concentration of an antimicrobial agent required to completely inhibit bacterial growth.[61] The findings from this study demonstrate that surface-stabilised Co_3O_4 NPs are effective antibacterial agents at relatively low doses, reinforcing their potential in combating antibiotic-resistant bacteria.[62] A novel colourimetric method utilising the oxidation-reduction indicator resazurin was

employed to determine MIC values. This technique allows for easy detection of bacterial inhibition through colour changes, with oxidised resazurin appearing blue and its reduced form turning pink or colourless. The antibacterial activity results revealed that Co_3O_4 NPs exhibited strong inhibitory effects against Staphylococcus aureus and *Enterococcus faecalis* (62.5 µl), moderate activity against *Pseudomonas aeruginosa* (125 µl), and lower activity against *Escherichia coli* (250 µl). The results indicate that Co_3O_4 NPs synthesised using *Achyranthes aspera* leaf extract exhibit potent antibacterial activity. The nanoparticles effectively inhibited bacterial growth through electrostatic interactions, ROS generation, and cell membrane disruption. Their efficacy against antibiotic-resistant strains highlights their potential as alternative antimicrobial agents. Further studies on their biocompatibility and mode of action will contribute to their development as a viable solution to combat bacterial infections. In keeping with SDG-3: Good Health and Well-Being, the antibacterial activity against Gram-positive and Gram-negative bacteria suggests possible uses in antimicrobial materials and healthcare. All of these enhancements help to strengthen the study's practical implications and offer proof of its value for sustainable development.



Fig.-8: Antibacterial Activity of Co_3O_4 NPs

Table-4: Antibacterial Activity of Co_3O_4 NPs

S.No.	Microorganisms/sample	Growth inhibition										
	Co_3O_4 NPs'	1000	500	250	125	62.5	31.2	15.6	7.8	STD10	Culture	DMSO
1	*Pseudomonas-aeruginosa*	-	-	-	-	+	+	+	+	-	+	+
2	*S- aureus*	-	-	-	-	-	+	+	+	-	+	+
3	*E. coli.*	-	-	-	+	+	+	+	+	-	+	+
4	*E. faecalis*	-	-	-	-	-	+	+	+	-	+	+

Table-5: MIC Value of Microorganisms

Microorganisms/sample	MIC Values (µl)
Pseudomonas aeruginosa (-ve)	125.0
Staphylococcus aureus (+ve)	62.5
Escherichia coli (-ve)	250.0
Enterococcus faecalis (+ve)	62.5

CONCLUSION

The Co_3O_4 NP's were prepared using the sol-gel route, using the natural reducing and stabilising agent *Achyranthes aspera* leaf extract. Structural and morphological investigations confirmed the formation of nanostructured Co_3O_4 nanoparticles in the cubic spinel phase. The functional groups responsible for nanoparticle synthesis and stability were confirmed by FTIR analysis. The synthesised material exhibited appropriate optical, morphological, elemental, and magnetic characteristics as evidenced by UV-DRS, SEM-EDS, TEM, and VSM studies. The green-produced Co_3O_4 nanoparticles exhibited good photocatalytic activity, achieving 62% degradation of methylene blue under photoreactor irradiation and 58% under direct sunlight in 60 min. Furthermore, nanoparticles demonstrated efficient antibacterial action against Gram-positive and Gram-negative bacterial strains, suggesting their multifunctional potential. The results showed that the green synthesis method is a straightforward, sustainable, and eco-friendly technique for the production of functional Co_3O_4 nanoparticles, which may be used for

wastewater treatment and antibacterial applications. Future research will concentrate on improving photocatalytic efficiency through material modification, investigating long-term stability and reusability, and researching the breakdown of real industrial effluent in real-world operating environments. Through sustainable dye removal from wastewater, green synthesis techniques, and the antibacterial efficacy of eco-friendly nanomaterials, this work advances the Sustainable Development Goals of the United Nations, particularly SDG-6(Clean Water and Sanitation), SDG-12 (Responsible Consumption and Production), and SDG-3 (Good Health and Well-Being). The findings open up a new avenue for the production of sustainable Co_3O_4 nanoparticles for use in medicine and the environment.

ACKNOWLEDGMENTS

The authors gratefully acknowledge the Department of Physics, Shrimathi Devkunvar Nanalal Bhatt Vaishnav College for Women, Chromepet, Chennai–600 044, Tamil Nadu, India, for providing the laboratory facilities and support during this research work.

CONFLICT OF INTERESTS

The authors declare that there is no conflict of interest regarding the publication of this manuscript. The authors alone are responsible for the content and writing of this article.

AUTHOR CONTRIBUTIONS

The present work is related to *SDG-9: Industry, Innovation, and Infrastructure*. All the authors contributed significantly to this manuscript, participated in reviewing/editing and approved the final draft for publication. The research profiles of the authors can be verified from their ORCID ids, given below:

K. Usha https://orcid.org/0009-0008-3130-7378
V. Ramesh https://orcid.org/0000-0003-0008-0218
P. Koteeswari https://orcid.org/0000-0002-6417-198X
D. V. Sridevi https://orcid.org/0000-0001-9061-7255
T. Kavitha https://orcid.org/0000-0001-7585-069X

Open Access: This article is distributed under the terms of the Creative Commons Attribution 4.0 International License (http://creativecommons.org/licenses/by/4.0/), which permits unrestricted use, distribution, and reproduction in any medium, provided you give appropriate credit to the original author(s) and the source, provide a link to the Creative Commons license, and indicate if changes were made.
Cite this article as: K. Usha *et al.*, *Rasayan J. Chem.*, 19(4), 2307-2319(2026), https://doi.org/10.31788/RJC.2026.1949953

REFERENCES

1. P.B. Chouke, T. Shrirame, A.K. Potbhare, A. Mondal, A.R. Chaudhary, S. Mondal, S.R. Thakare, E. Nepovimova, M. Valis, K. Kuca, R. Sharma and R.G. Chaudhary, *Materials Today Advances*,**16**, 100314(2022), https://doi.org/10.1016/j.mtadv.2022.100314
2. P. Chelliah, S.M. Wabaidur, H.P. Sharma, M.J. Jweeg, H.S. Majdi, M.M.R. Al Kubaisy, A. Iqbal and W.C. Lai, *Water*, **15**, 910(2023), https://doi.org/10.3390/w15050910
3. M.S. Chavali and M.P. Nikolova, *SN Applied Sciences*, **1**, 607(2019), https://doi.org/10.1007/s42452-019-0592-3
4. G. Ayyakannu Sundaram, R. Kanniah and K. Anbalagan, *Inorganic Chemistry Communications*,**189**, 116702 (2026), https://doi.org/10.1016/j.inoche.2026.116702
5. G. Ayyakannu Sundaram, R. Kanniah, K. Anbalagan, K. Kulandaivelu and H. Valdés, *Catalysts*,**14(3)**, 169 (2024), https://doi.org/10.3390/catal14030169
6. M.S. Hassan, T. Amna and M.S. Khil, *Ceramics International*, **40**, 423(2014), https://doi.org/10.1016/j.ceramint.2013.06.043
7. D. Gawande, S. Barewar, J. Taksande, M. Umekar, B. Ghule, B. Taksande and N. Kotagale, *Journal of Traditional Complementary Medicine*, **12**, 545(2022), https://doi.org/10.1016/j.jtcme.2022.06.001
8. X. He, X. Wang, J. Fang, Y. Chang, N. Ning, H. Guo and X. Huang, *Journal of Ethnopharmacology*, **203**, 260(2017), https://doi.org/10.1016/j.jep.2017.03.035
9. S.T. Al-Asadi and F.F. Al-Qaim, *Eurasian Chemical Communication*, **5**, 794(2023), https://doi.org/10.22034/ecc.2023.1976543

10. M.M. Mankilik, I.Y. Longdet and C.D. Luka, *Journal Basic Applied Zoology*, **82**, 1(2021), https://doi.org/10.1186/s41936-021-00215-4
11. B.R. Goyal, R.K. Goyal and A.A. Mehta, *Pharmacognosy Reviews*, **1**, 143(2007)
12. E.K. Elumalai, N. Chandrasekaran, T. Thirumalai, C. Sivakumar, S.V. Therasa and E. David, *International Journal of Pharm Tech Research*, **1**, 1576(2009)
13. K. Khandelwal, Practical Pharmacognosy, *Pragati Books Pvt. Ltd.*, 78(2008)
14. H. Boumeriame, E.S. Da Silva, A.S. Cherevan, T. Chafik, J.L. Faria and D. Eder, *Journal of Energy Chemistry*, **64**, 406(2022), https://doi.org/10.1016/j.jechem.2021.09.038
15. Sani, A. Murad, D. Hassan, G.M. Channa, A. El-Mallul and D.I. Medina, *Environment Science and Pollution Research*, **30**, 20736(2023), https://doi.org/10.1007/s11356-022-23691-7
16. M.T. Alam, M.M. Karim and S.N. Khan, *Journal of Scientific Research*, **1**, 393(2009), https://doi.org/10.3329/jsr.v1i2.1079
17. Waris, M. Din, A. Ali, S. Afridi, A. Baset, A.U. Khan and M. Ali, *Open Life Science*, **16**, 14(2021), https://doi.org/10.1515/biol-2021-0003
18. M. Salavati-Niasari and A. Khansari, *Comptes Rendus Chiminie*, **17**, 352(2014), https://doi.org/10.1016/j.crci.2013.10.006
19. C.I. Priyadharsini, G. Marimuthu, T. Pazhanivel, P.M. Anbarasan, V. Aroulmoji, V. Siva and L. Mohana, *Journal of Sol-Gel Science and Technology*, **96**, 416(2020), https://doi.org/10.1007/s10971-020-05393-x
20. D. Saravanakkumar, S. Sivaranjani, K. Kaviyarasu, A. Ayeshamariam, B. Ravikumar, S.Pandiarajan and M. Maaza, *Journal of Semiconductors*, **39**, 033001(2018), https://doi.org/10.1088/1674-4926/39/3/033001
21. N.M. Ishak, S.K. Kamarudin and S.N. Timmiati, *Materials Research Express*, **6**, 112004(2019), https://doi.org/10.1088/2053-1591/ab3f10
22. R. Bhargava, S. Khan, N. Ahmad and M.M.N. Ansari, *AIP Conference Proceedings*, **1953**, 030214(2018), https://doi.org/10.1063/1.5032483
23. S. Naz, S. Kiran, T. Gulzar and T. Farooq, *Global NEST Journal*, **26**, 1(2024), https://doi.org/10.30955/gnj.005432
24. M. Salavati-Niasari and A. Khansari, *Comptes Rendus Chimie*, **17**, 352(2014), https://doi.org/10.1016/j.crci.2013.10.006
25. C.T. Anuradha and P. Raji, *Journal of Molecular Structure*, **1262**, 133065(2022), https://doi.org/10.1016/j.molstruc.2022.133065
26. P. Chelliah, S.M. Wabaidur, H.P. Sharma, M.J. Jweeg, H.S. Majdi, M.M.R. Al Kubaisy and W.C. Lai, *Water*, **15**, 910(2023), https://doi.org/10.3390/w15050910
27. O.A. Fouad, S.A. Makhlouf, G.A. Ali and A.Y. El-Sayed, *Materials Chemistry and Physics*, **128**, 70(2011), https://doi.org/10.1016/j.matchemphys.2011.02.012
28. B. Seyyedi and B. Shakhseh, *Alexandria Engineering Journal*, **61**, 6919(2022), https://doi.org/10.1016/j.aej.2021.12.042
29. R. Varadhaseshan, S.M. Sundar and C. Prema, *The European Physical Journal- Applied Physics*, **66**, 10602(2014), https://doi.org/10.1051/epjap/2014130453
30. M. Naseri, A. Dehzangi, H.M. Kamari, A. See, M. Abedi, R. Salasi and B.Y. Majlis, *Metals*, **6**, 181(2016), https://doi.org/10.3390/met6080181
31. R. Bhargava, S. Khan, N. Ahmad and M.M.N. Ansari, *AIP Conference Proceedings*, **1953**,030214(2018), https://doi.org/10.1063/1.5032483
32. N.O. Mulya Dewi, Y. Yulizar and D.O.B. Apriandanu, *IOP Conference Series: Materials Science and Engineering*, **509**, 012105(2019), https://doi.org/10.1088/1757-899X/509/1/012105
33. M.B. Muradov, S.J. Mammadyarova, G.M. Eyvazova, O.O. Balayeva, G. Aliyeva, I. Hasanova and M.I. Abdullayev, *RSC Advances*, **14**, 1082(2024), https://doi.org/10.1039/D3RA07891A
34. N. Naveenkumar, A. Abhishek, P. Umadevi, B. Neppolian, S.K. Mukaddar, Ibrar, T.C. Sabari Girisun and V. Ramesh, *Ceramics International*, **51(24)**, 42139(2025), https://doi.org/10.1016/j.ceramint.2025.06.429
35. P. Umadevi, D.V. Sridevi, N. Naveenkumar, M. Abith, T.C. Sabari Girisun and V. Ramesh, *Journal of Alloys and Compounds*, **1008**, 176683(2024), https://doi.org/10.1016/j.jallcom.2024.176683
36. P. Umadevi, K.T. Ramya Devi, D.V. Sridevi, Suresh Perumal and V. Ramesh, *Materials Science and Engineering: B*, **286**, 116018(2022), https://doi.org/10.1016/j.mseb.2022.116018

37. C.R. Dhas, R. Venkatesh, K. Jothivenkatachalam, A. Nithya, B.S. Benjamin, A.M.E. Raj and C. Sanjeeviraja, *Ceramics International*, **41**, 9301-9308(2015), https://doi.org/10.1016/j.ceramint.2015.03.235
38. A.S. Vijayanandan and R.M. Balakrishnan, Journal of Environmental Management, **218**, 442(2018), https://doi.org/10.1016/j.jenvman.2018.04.058
39. D. Pradhan, E. Falletta and S.K. Dash, *Optical Materials*, **135**, 113368(2023), https://doi.org/10.1016/j.optmat.2022.113368
40. S. Haq, F. Abbasi, M.B. Ali, A. Hedfi, A. Mezni, W. Rehman and H. Shaheen, *Materials Research Express*, **8**, 075009(2021), https://doi.org/10.1088/2053-1591/ac0e6f
41. G. Patel, A.R. Patel, G. Maity, S. Das, S.P. Patel and S. Banerjee, *Current Research in Green Sustainable Chemistry*, **5**, 100258(2022), https://doi.org/10.1016/j.crgsc.2022.100258
42. B. Meenatchi, V.S. Lakshmi, A. Manikandan, V. Renuga, A. Sharmila, K.R. Nandhine Deve and S.K. Jaganathan, *Journal of Inorganic Organometallic Polymers and Materials*, **27**, 446(2017), https://doi.org/10.1007/s10904-016-0527-3
43. S. Xu, Y. Ma, Y. Xu, X. Sun, B. Geng, G. Zheng and Z. Dai, *Nanoscale Research Letters*, **9**, 545(2014), https://doi.org/10.1186/1556-276X-9-545
44. T. Özkaya, A. Baykal, M.S. Toprak, Y. Koseoğlu and Z. Durmuş, *Journal of Magnetism and Magnetic Materials*, **321**, 2145(2009), https://doi.org/10.1016/j.jmmm.2009.02.075
45. V. Vasanthi, A. Shanmugavani, C. Sanjeeviraja and R.K. Selvan, *Journal of Magnetism and Magnetic Materials*, **324**, 2100(2012), https://doi.org/10.1016/j.jmmm.2012.01.046
46. R.M. Mohamed, I.A. Mkhalid, E.S. Baeissa and M.A. *Al-Rayyani, Journal of Nanotechnology*, **2012**, 329082(2012), https://doi.org/10.1155/2012/329082
47. A.B. Vennela, D. Mangalaraj, N. Muthukumarasamy, S. Agilan and K.V. Hemalatha, *International Journal of Electrochemical Science*,**14**, 3535(2019), https://doi.org/10.20964/2019.04.32
48. S. Hemamalini and R. Manimekalai, *Bulletin of Materials Science*, **44**, 154(2021), https://doi.org/10.1007/s12034-021-02432-7
49. P.D. Sarvalkar, A.S. Jamadar, A.B. Magdum, P.K. Pawar, J.B. Yadav, M.S. Nimbalkar and K.K.K. Sharma, *Results in Engineering*, **22**, 102094(2024), https://doi.org/10.1016/j.rineng.2024.102094
50. Bibi, N. Nazar, M. Iqbal, S. Kamal, H. Nawaz, S. Nouren and M. Abbas, *Advanced Powder Technology*, **28**, 2035(2017), https://doi.org/10.1016/j.apt.2017.05.021
51. K.M. Gendo, R.F. Bogale and G. Kenasa, *ACS Omega*, **9**, 1(2024), https://doi.org/10.1021/acsomega.4c01234
52. V. Gupta, V. Kant, A.K. Sharma and M. Sharma, *Journal of Indian Chemical Society*, **99**,100533(2022), https://doi.org/10.1016/j.jics.2022.100533
53. T.J. Hossain, *European Journal of Microbiology and Immunology*, **14**, 97(2024), https://doi.org/10.1556/1886.2024.00012
54. J.S. Ajarem, S.N. Maodaa, A.A. Allam, M.M. Taher and M. Khalaf, *Journal of Cluster Science*, **32**, 1(2021), https://doi.org/10.1007/s10876-020-01887-y
55. N.E. Eleraky, A. Allam, S.B. Hassan and M.M. Omar, *Pharmaceutics*, **12**, 142(2020), https://doi.org/10.3390/pharmaceutics12020142
56. A.M. Ahmed, M.F. Al Marjani and A.M. Rheimah, *Bionatural*, **8**, 78(2023), https://doi.org/10.55873/BN.2023.8.1.78
57. Syed, A.M. Elgorban, A.H. Bahkali and N.S. Zaghloul, *Colloid Interface Science Communication*, **44**, 100467(2021), https://doi.org/10.1016/j.colcom.2021.100467
58. L. Wang, C. Hu and L. Shao, *International Journal of Nanomedicine*, **12**, 1227(2017), https://doi.org/10.2147/IJN.S121956
59. N. Mubraiz, A. Bano, T. Mahmood and N. Khan, *Agronomy*, **11**, 1607(2021), https://doi.org/10.3390/agronomy11081607
60. G. Pandey, C.V. Rao, S.S. Gupta, K.K. Verma and M. Singh, *European Journal of Medicinal Plants*, **4**, 695(2014), https://doi.org/10.9734/EJMP/2014/8547
61. M. Balouiri, M. Sadiki and S.K. Ibnsouda, *Journal of Pharmaceutical Analysis*, **6**, 71(2016), https://doi.org/10.1016/j.jpha.2015.11.005
62. T. Ameh, K. Zarzosa, J. Dickinson, W.E. Braswell and C.M. Sayes, *Frontiers in Microbiology*, **14**, 1119550(2023), https://doi.org/10.3389/fmicb.2023.1119550

[RJC-9953/2026]